4.5.3. Cloud and Aerosol Effect on O_3 retrieval

(1) Cirrus cloud and aerosol contribution to the effective air mass factor

The cirrus cloud and aerosol contributions to the effective air-mass factor are summarized in Table 4-10. Figure 4-43 schematically illustrates the effect of thin clouds. The effective optical path is not affected by thin clouds since forward scattering is much stronger than backward scattering. The simulated air-mass factor of the Figure 4-43 geometry is 1.96 if the optical thickness is 0.3, which is close to cloud-free conditions.

Table 4-10. Cirrus cloud and aerosol contribution on effective air mass factor.

	Cirrus	Tropospheric Aerosol
Typical altitude	High	Relatively low
Phase function model dependency	Relatively small	Type dependent
Spectral characteristics	White	Type dependent
Contribution for effective airmass	Moderate	Small

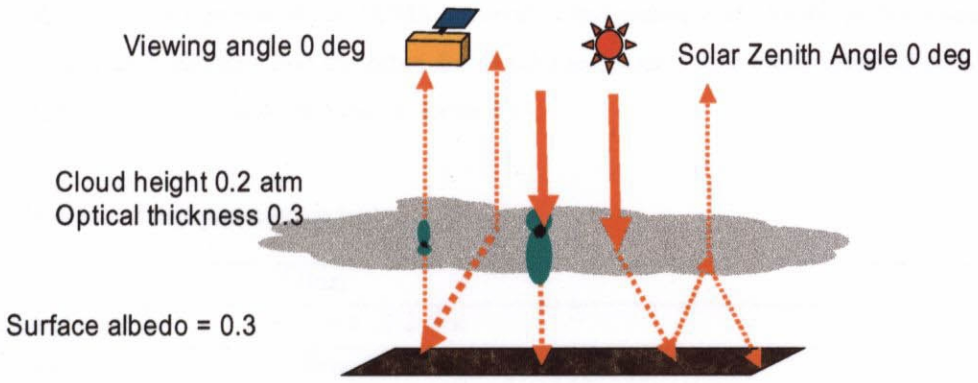

Figure 4-43. Schematics of the forward scattering effect on the effective air-mass factor.

(2) Pair values for aerosols

Backward scattering (reflection) is much less than forward scattering in the presence of small clouds or aerosols. Therefore, a thin cloud or aerosol does not affect the total O_3 retrieval much. Figure 4-44 shows the forward calculation of the pair values for absorbing and non-absorbing aerosols. The pair N-values are not affected much in either case. Characterization of different types of aerosols is discussed in chapter 4.6.

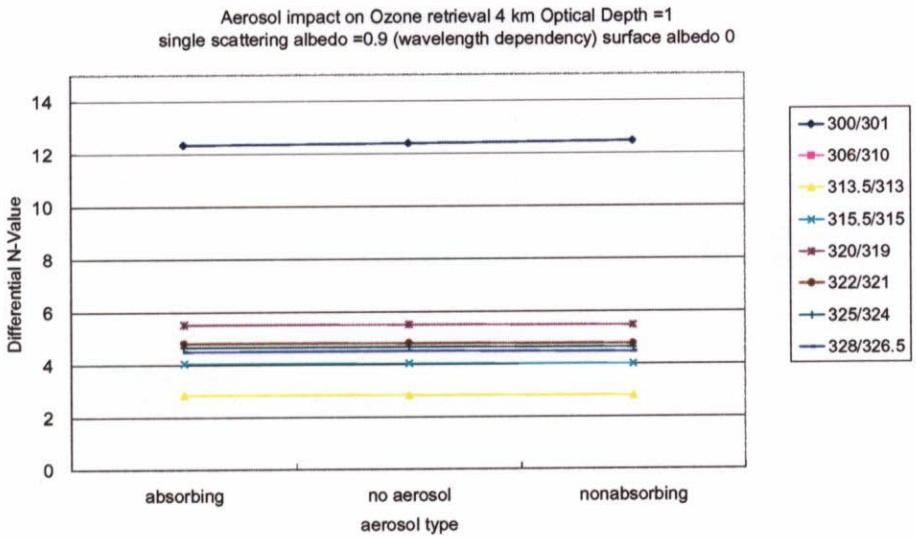

Figure 4-44. Aerosol effect on the ratio of O_3 sensitive and insensitive pairs.

4.5.4. Cloud and Aerosol Correction using Look-up Tables

Two kinds of LUT are prepared for TOMS retrieval in the presence of clouds, as discussed in Chapter 2; one is for cloud-free conditions and the other for cloud conditions. The cloud effect of middle altitudes must be corrected. The LUT items are listed in Table 4-11.

Table 4-11. Items for look up tables.

Item	Step
Cloud height (atm)	1, 0.6 , 0.2 atm
O_3 profiles	Total O_3: 225-425 (50 DU step) Vertical profile: 6 profiles Total 5 by 6 models
Geometries	Solar zenith angle: 0, 15, 30, 40, 50, 60, 70, 75, 80, 85 degrees Viewing angle: 0, 15, 30, 40, 50, 60 degrees

4.6. Aerosol Retrieval

4.6.1. Aerosol Measurements in the UV region

(1) Aerosol retrieved by TOMS

TOMS measured the global aerosol distribution from a satellite for the first time. Both land and ocean aerosol can be measured using the UV spectra. Figure 4-45 contains the monthly average observed aerosol index (optical depth equivalent). The absolute value was not calibrated, and the stripes of the orbit cannot be removed due to the limitation of the TOMS spectral channels. Figure 4-46 schematically illustrates previous aerosol observation and the new retrieval algorithm using UV and O_2 *A* band spectra.

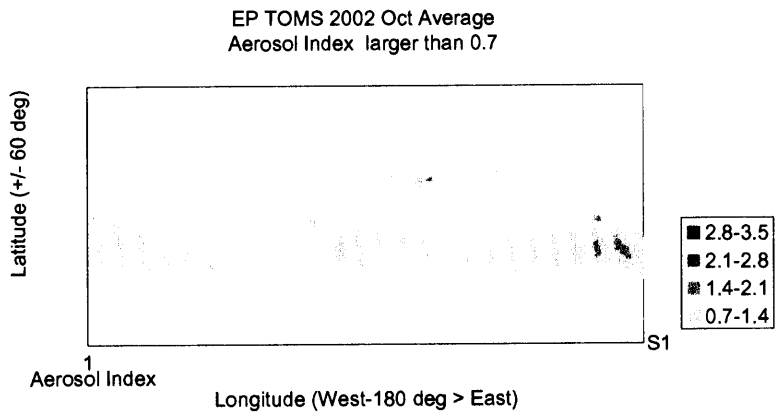

Figure 4-45. Global distribution of the absorption aerosol index measured by EP TOMS. The data is the monthly average of October 2002.

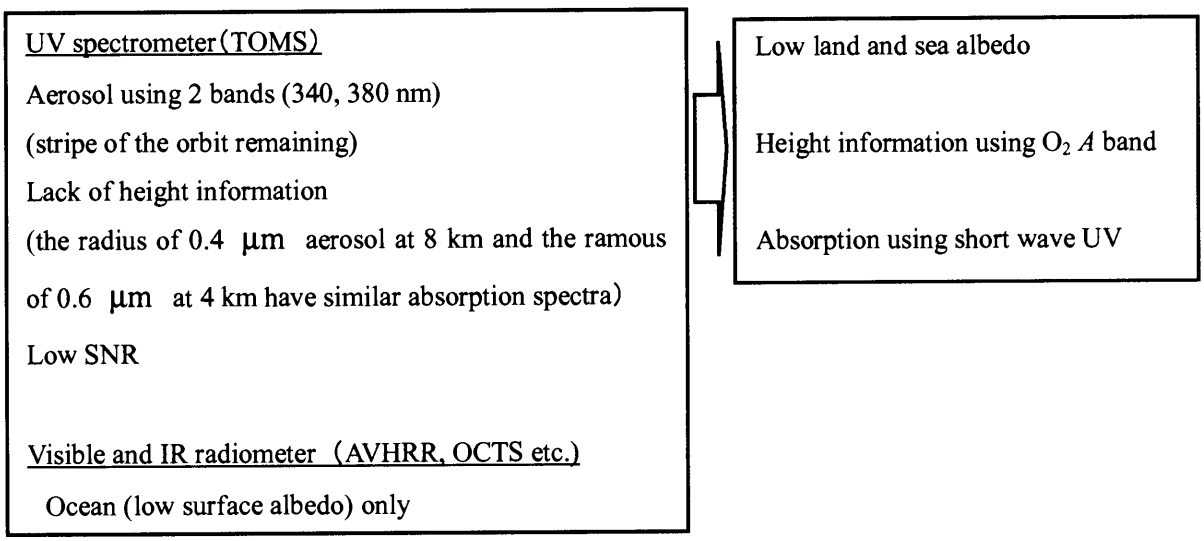

Figure 4-46. Previous aerosol observations and new retrieval algorithm using UV and O_2 *A* band spectra.

4.6.2. Simulation Model (Forward Calculation)

The following is an equation to simulate the radiative transfer of aerosol in UV region to estimate the Mie and Rayleigh scattering effect. The multiple scattering is omitted to estimate the rough order of magnitude. The first and second parts are the Rayleigh scattering above and below the aerosol layer, and the last part is the Mie scattering effect of the aerosol. The simulated spectral radiance can be described as,

$$I_\lambda = \frac{1}{4\pi} F_\lambda \beta_\lambda P(\cos\theta_0)\left(\int_0^{P_a} s_1 \exp\left[-s_2(\alpha_\lambda x_p + \beta_\lambda p)\right] dp + \exp(-s_2\tau(1-\varpi_0))\int_{P_a}^{1} s_1 \exp\left[-s_2(\alpha_\lambda x_p + \beta_\lambda p)\right] dp\right), \quad (4\text{-}16)$$
$$+\frac{1}{4\pi} F_\lambda \varpi_0 \left(1-(1-P_{hg}(\cos\theta_0))\exp(-\gamma s_1\tau)\right)\left(1-\exp(-s_1\tau)\right)\exp\left[-s_2(\alpha_\lambda x_p + \beta_\lambda P_a)\right]$$

where ϖ_0 is the single scattering albedo, P_a is the pressure of the aerosol layer, and $P(cos\theta_0)$ and $P_{hg}(cos\theta_0)$ are phase function of Rayleigh scattering and Mie scattering (Henyey and Greenstein phase function), respectively. Figure 4-47 portrays the spectral characteristics of the Rayleigh scattering coefficient, optical thickness, and single-scattering albedo used in the model calculation.

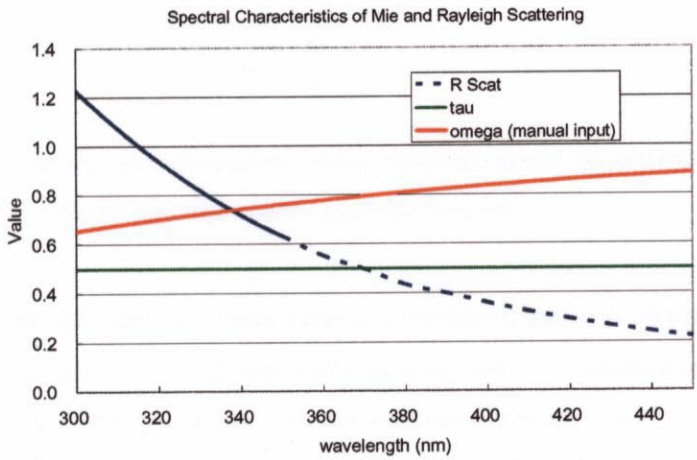

Figure 4-47. The spectral characteristics of Rayleigh scattering coefficient, optical thickness and single scattering albedo in the model calculation.

4.6.3. Aerosol Model

The advantage of continuous UV spectral measurements was investigated to study the feasibility of land and tropospheric aerosol retrieval.

(1) Phase function

The Henyey and Greenstein model was used as the conventional phase function of Mie scattering [*Henyey and Greenstein*, 1941]. Figure 4-48 depicts an example of the Henyey and Greenstein phase function model for different asymmetry factors together with the Rayleigh scattering phase function.

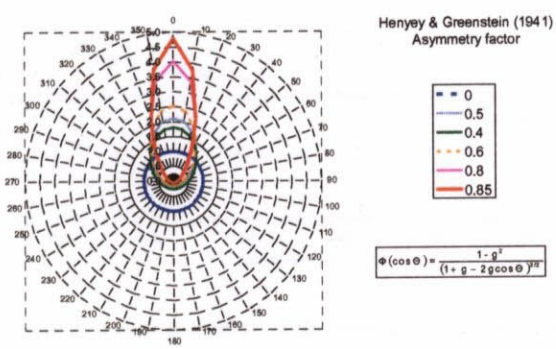

(a)

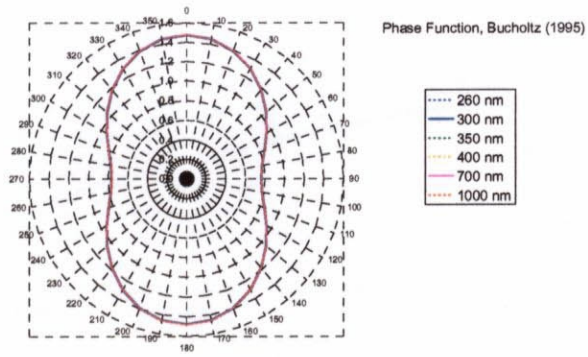

(b)

Figure 4-48. Henyey and Greenstein phase function model of different asymmetry factors compared with (b) Rayleigh scattering phase function.

(2) Single-scattering albedo and spectral characteristics of aerosol absorption

Typical aerosol types such as mineral dust, carbonaceous, and, UV nonabsorbent (liquid sulfate) were modeled. Absorption in the shorter UV region is strong and sensitive to the size of the UV absorption aerosol, as discussed in section 4.5. The absolute radiometric response must be carefully calibrated since the shorter-wavelength region spectra itself is weak and absorbed by the O_3.

Absorption by the aerosol can be calculated as follows;

$$I / I_0 = exp(-4\pi n_{IM}(\lambda) r / \lambda), \qquad (4\text{-}17)$$

where $n_{im}(\lambda)$ is the spectral characteristics of the imaginary part of the refraction index, r is the radius of the aerosol article, and λ is the wavelength.

Figure 4-49 shows the imaginary part of the spectral model of the dust aerosol refraction index used in this model calculation [*Patterson et al.*, 1977 and *Torres et al.*, 2002.]. Figure 4-50 and Figure 4-51 depict the spectral characteristics of the single-scattering albedo of mineral dust and carbonaceous aerosols of different size models.

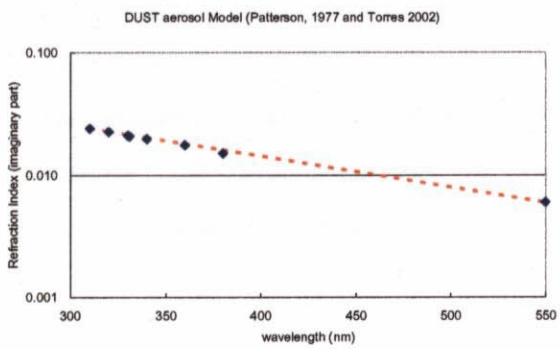

Figure 4-49. Imaginary part spectral model of the refraction index of dust aerosol.

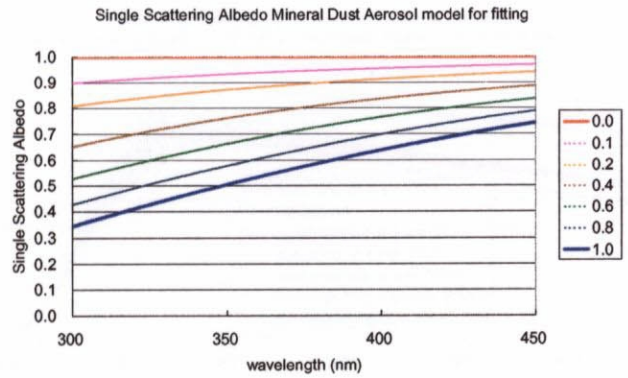

Figure 4-50. Spectral characteristics of the single-scattering albedo of mineral dust aerosol of different size models.

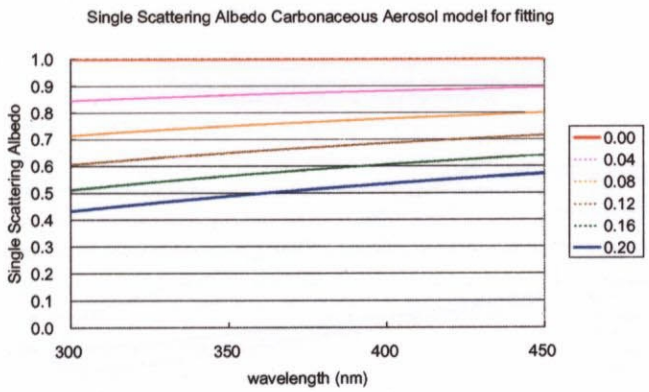

Figure 4-51. Spectral characteristics of the single-scattering albedo of carbonaceous aerosol of different size models.

4.6.4. Sensitivity to Aerosol Characteristics (Forward Calculation)

Figure 4-52 presents simulated spectral characteristics of Earth albedo of different aerosol types measured from orbit and Figure 4-53 displays their ratio to the aerosol-free conditions. Figure 4-54 shows the simulated Earth albedo of dust and carbonaceous aerosols located at an altitude of 4 km. Figure 4-55 depicts the simulated Earth albedo of dust aerosols: the radii of 0.4 and 0.6 μm, optical thickness of 0.5, and the heights of 4 km and 8 km. The simulated values of aerosol of 0.4 μm -radius at 8 km and one the 0.6 μm -radius aerosol at 4 km are similar. The results demonstrate that the aerosol size and optical thickness cannot be distinguished without the aerosol height information.

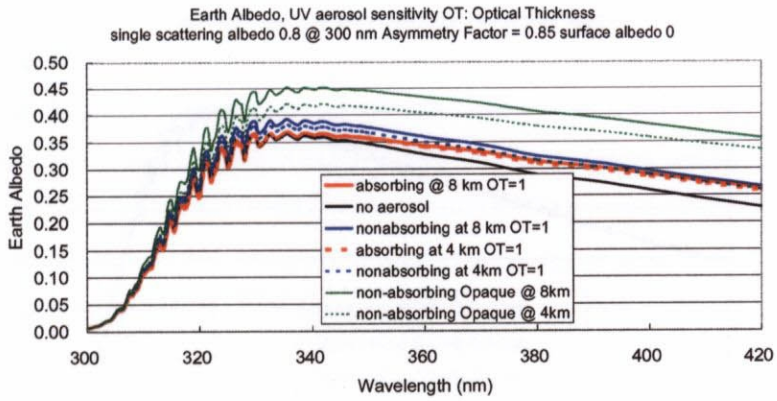

Figure 4-52. Simulated spectral characteristics of the earth albedo of different aerosol types measured from orbit.

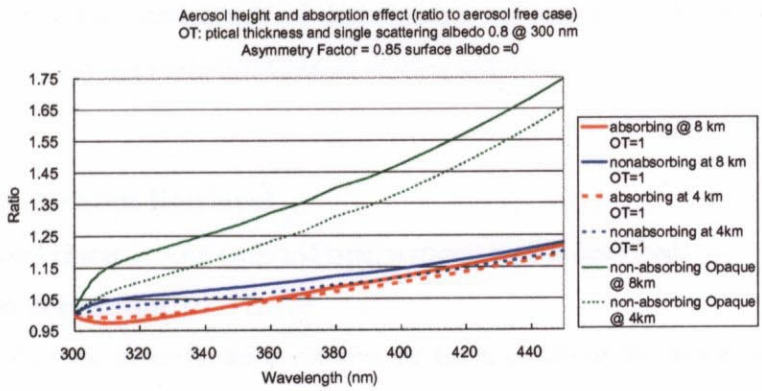

Figure 4-53. The ratio of the simulated spectral characteristics of the earth albedo of different aerosol types.

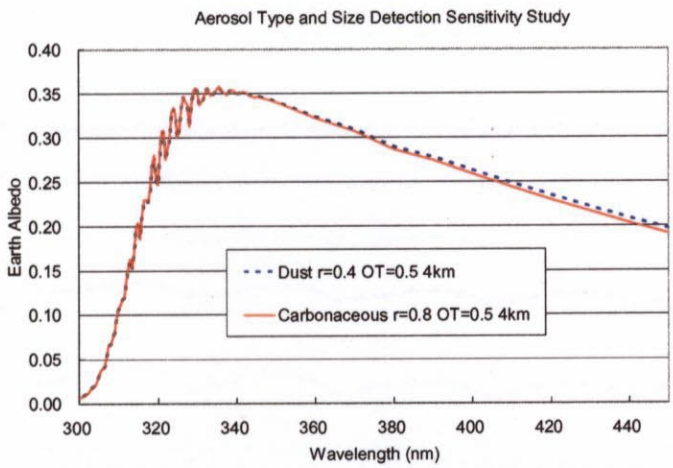

Figure 4-54. Simulated earth albedo of dust and carbonaceous aerosols located at the altitude of 4 km.

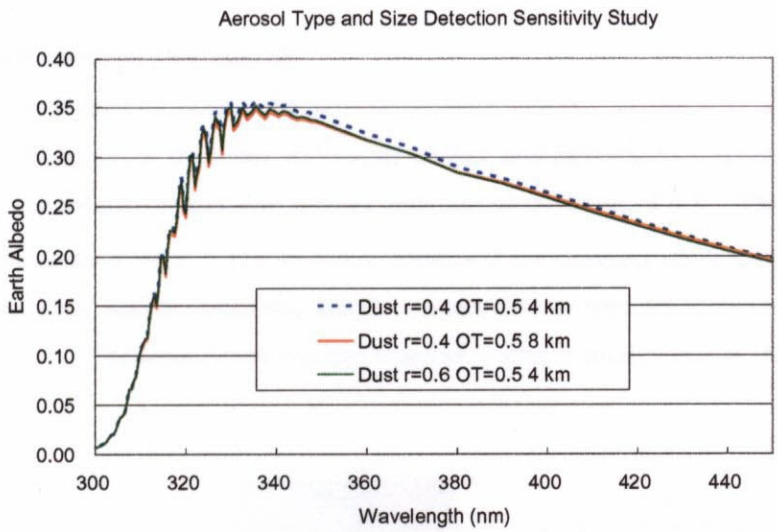

Figure 4-55. Simulated earth albedo of dust aerosols: the radius of 0.4 and 0.6 μm, optical thickness of 0.5 and the height location of 4 km and 8 km.

4.6.5. Aerosol Characteristics Retrieval

In this section, aerosol characteristics (size and type) retrieval flow is described.

(1) Ozone absorption correction

The absorption by O_3 must be corrected to retrieve the Earth albedo of the shorter wavelength region. The earth albedo of O_3 insensitive channels can be corrected with minimal errors by using the information of the retrieved total O_3 amount from the measured data. Figure 4-56 presents the estimated optical depth using eight O_3 insensitive channels and variations between 30 different total O_3 and vertical profile models; the worst case has a 0.002 Earth albedo estimation error.

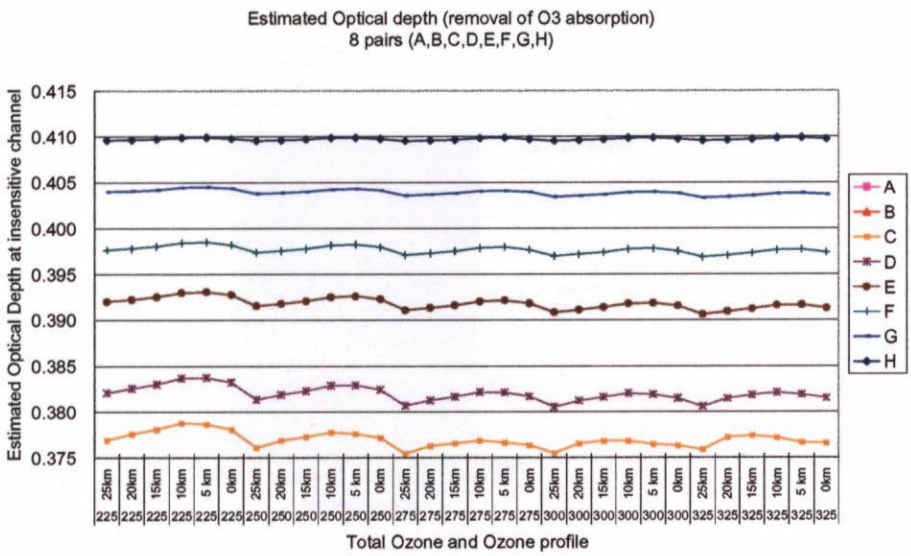

Figure 4-56. The estimated optical depth using O_3 insensitive channels of 7 pairs.

(2) Grid search method (Retrieval)

The grid search method is used for aerosol characterization. Figure 4-57 and Figure 4-58 show the fitting process of both optical thickness and radius of dust and carbonaceous aerosols, respectively. In this case, true values are 0.4 μm radius dust aerosol with optical thickness of 0.5. The fitting used the two sets of tables: dust and carbonaceous. The deviation remains if the incorrect aerosol model is applied for fitting. Therefore, aerosol size, optical thickness, and absorption aerosol type are retrieved with the LUT of three unknown parameters. The aerosol type can be classified if error is smaller than 0.1%.

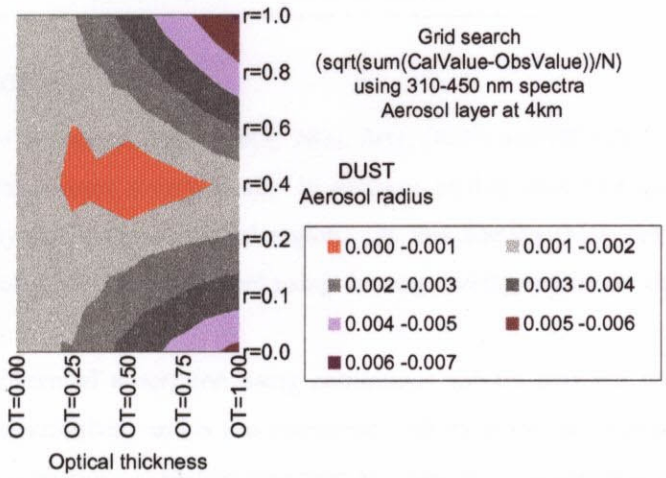

Figure 4-57. The sum of the earth's albedo deviation at band 1, which is minimized in the fitting process to determine the aerosol optical thickness and dust aerosol radius for the dust aerosol measurement.

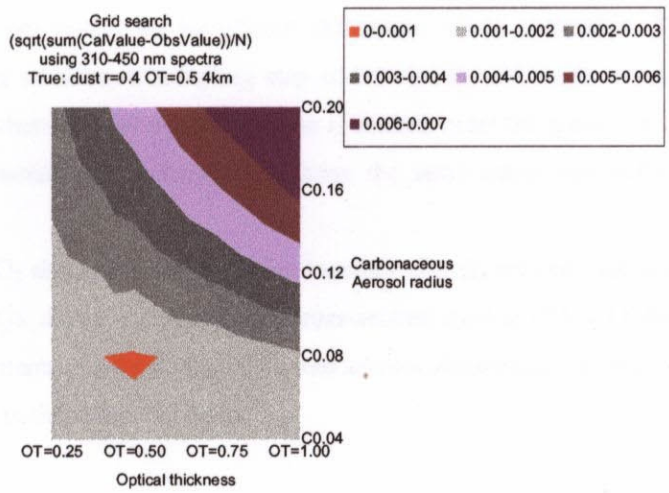

Figure 4-58. The same as Figure 4-57 except for using the carbonaceous aerosol model for dust aerosol fitting.

(3) Retrieval error estimation

The major error sources and expected accuracy are summarized in Table 4-12. Aerosol retrieval requires accurate radiometric calibration; a combination of aerosol reflection data near O_2 *A* band and *a priori* information about the type is useful.

Table 4-12. The major error sources and expected accuracy.

Error level	Error Effect
Radiometric error: 0.1 %	0.2 μm error in dust aerosol radius and 0.3 error in optical thickness

4.7. Air Pollution Monitoring

The absorption of minor trace molecules, such as SO_2, NO_2, BrO, OClO, and HCHO, is weak compared with O_3 and aerosol because the total amount is very small. In addition, as they have fine spectral structures, they can be retrieved independently in the local spectral region. In this section, NO_2 retrieval is mainly discussed and the retrieved results of ground measurement using the engineering model are shown in Chapter 5.

NO_2 can be retrieved by differential absorption using continuous spectra between 432 and 452 nm, where NO_2 absorption has sufficient sensitivity and is less interfered with by other constituents. Figure 4-59 depicts the HITRAN 2000 NO_2 absorption cross-section data base at 294K in the longer-wavelength region of the engineering model and band 2 spectral region of the flight model. Figure 4-60 illustrates the simulated spectra by convoluting the NO_2 absorption cross section with an instrument function of FWHM = 0.25, 0.5, 1.0, and 2.0 nm. If we tune the defocus position to maximize the spectral resolution in the UV region, the spectral resolution around 440 nm becomes about twice as wide (FWHM = 1.0 nm) as the one in the shorter-wavelength region due to the nature of the Fastie-Ebert type spectrometer. The results indicate that FWHM = 0.25, 0.5, and 1.0 nm reveal no significant difference, while FWHM = 2.0 nm exhibits less sensitivity than the others. In addition, a sampling step of 0.5 nm is sufficiently robust to reconstruct the spectral feature of NO_2, even when the wavelength position is shifted under the space environment Therefore, the instrument has sufficient sensitivity to detect NO_2 using the same optics and defocus position without sacrificing SNR.

Figure 4-61 depicts an SO_2 absorption cross-section together with O_3 between 306 and 320 nm [*McGee et al.*, 1987]. Figure 4-62 displays shows the absorption cross-section models of H_2CO, BrO, and OClO. The absorption of the minor constituents is the residual of O_3 and aerosol absorption. It can be extracted by fitting the model-calculated spectrum to the measured one.

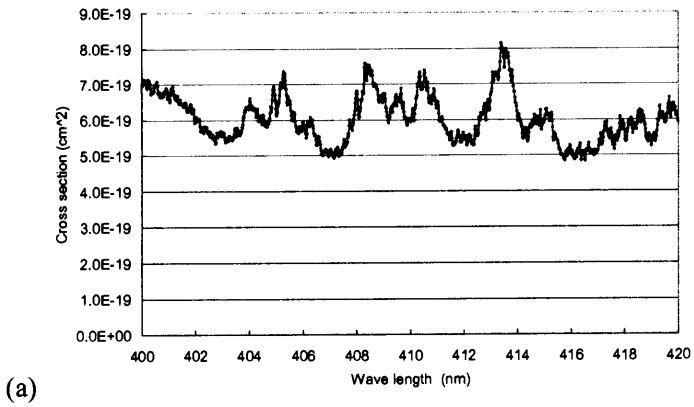

(a)

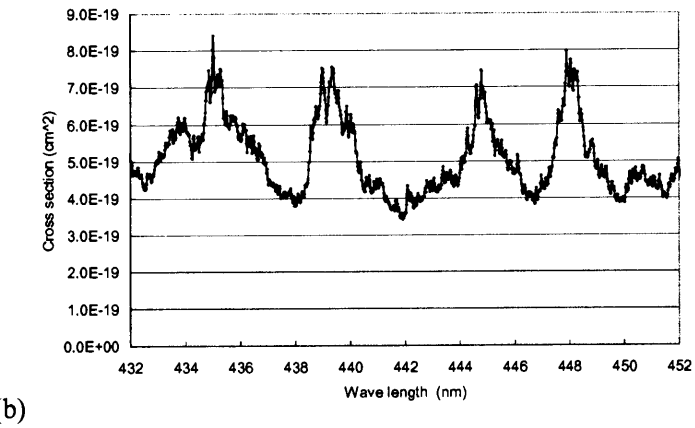

(b)

Figure 4-59. HITRAN 2000 NO_2 absorption cross section data base at 294 K with 0.965 cm^{-1} step: (a) 400-420 nm spectral range and (b) 432-452 nm spectral range.

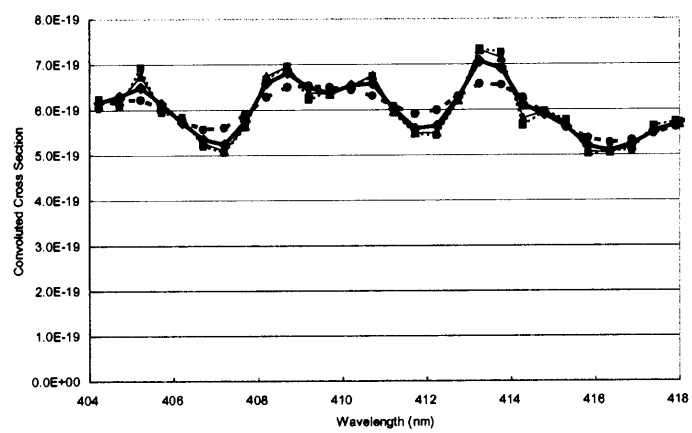

(a)

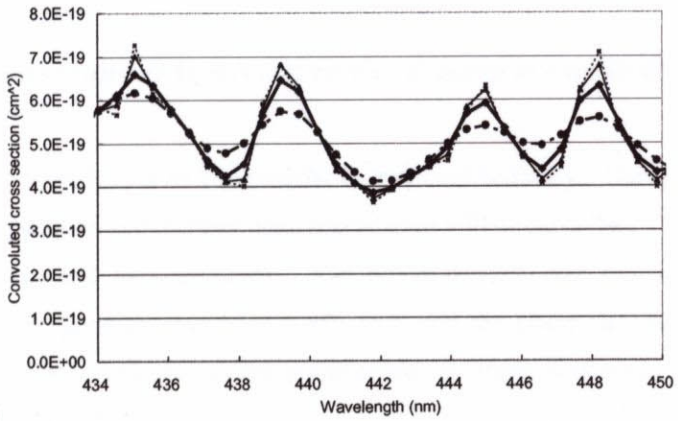

(b)

Figure 4-60. Convoluted absorption cross section assuming Gaussian shape instrument function of FWHM = 0.25 (dotted line), 0.5 (solid line), 1.0 (bold line), and 2.0 nm (dash dotted line): (a) 400-420 nm spectral range and (b) 432-452 nm spectral range..

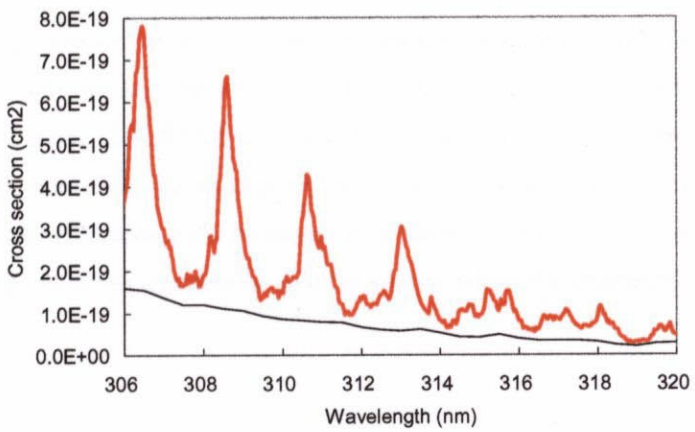

Figure 4-61. SO_2 absorption cross section model (bold line) together with O_3 (solid line).

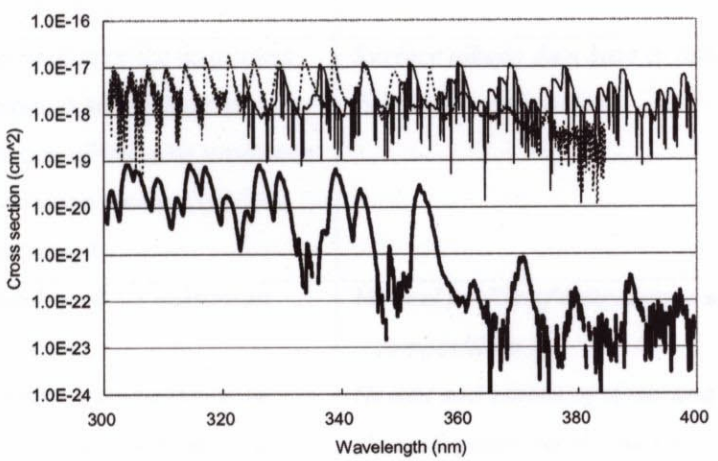

Figure 4-62. Cross section model of H_2CO at 293K (bold line), BrO at 243K (dotted line), and OClO at 253K (solid line).

4.8. Retrieval Accuracy

4.8.1. Error type and its transfer in overall retrieval accuracy analysis

(1) Error source

One of the scientific objectives is to improve the O_3 retrieval accuracy. Using the pair method, several errors such as response degradation and diffuser plate degradation will be cancelled. The retrieval error sources are both model calculations and measurements. The physical parameter errors come mainly from the absorption cross-section, the Rayleigh scattering coefficient, and the phase function inaccuracy. The error sources of the radiative transfer calculation are polarization, multiple scattering, O_3 vertical profile, and reflection at the surface and cloud tops.

The atmospheric components measurements are very simply modeled as follows. Predicted error sources of each coefficients and constants are summarized in Table 4-13.

$$Y = a\,exp(-bX + c) + d \quad (4\text{-}18)$$

For measurements, there are two kinds of errors: systematic error and random error. Systematic error is mainly from the slit function model error, the response degradation on board and wavelength shift. Random error is mainly due to the detector and pre-amplifier noise. Averaging the measured data over the spectra and space can reduce random error. The STAR code will be upgraded from a scalar model to a vector model to consider polarization. In this case, the absorption cross section inaccuracy and the estimation error of the effective center wavelength will become the dominant error source. In the case of the O_3 retrieval, the surface albedo and aerosol estimation errors can also be an error source, while the interference of minor constituents is small enough.

Table 4-13. Error sources of the retrieval.

Coefficients and constants	Systematic error from measurements	Systematic error from model
a	Degradation of the instrument response and diffuser plates Variation of the solar irradiance Polarization sensitivity of the instrument	***Surface albedo data base*** or estimation Polarization calculation
b	Instability of the instrument function Geometry parameters (solar zenith angle, viewing angle)	***Vertical profile of temperature and atmospheric compositions*** ***Height and albedo of cloud and aerosol*** Physical parameter (Cross section, Fraunhofer lines) Multiple scattering Radiative transfer calculation
c	-	***Other constituents interference***
d	Offset of the instrument signal	-

Bold Italic letter indicates the items that can no be minimized by calibration and validation..

(2) Accuracy improvement using the retrieved geophysical parameters (stratospheric aerosol and surface albedo)

The ADEOS TOMS algorithm retrieves the surface albedo without considering aerosol. The calculated Earth albedo becomes 0.396 when we assumed that the stratospheric aerosol transmittance and surface albedo were 0.8 and 0.2 (true value), which are an extreme case. The retrieved value of the surface albedo is 0.372 (86 % error) without considering aerosol. The upwelling and downwelling flux calculation includes about 23% errors which is equal to a 10% error in total O_3 estimation using 321 nm spectra. The retrieved error of total O_3 is about 5% even if the estimated aerosol includes errors of 10%, which is lower than the retrieval error when aerosol is not considered. The above sensitivity study demonstrates that the accuracy of the polar region total O_3 retrieval is improved by including stratospheric aerosol in model calculation.

(3) Validation

For the total O_3 and troposphere O_3 retrieval, the vertical profile must be appropriately modeled for the look-up table calculation as discussed above. Validation using instruments other than the UV polychromator itself is the most comprehensive method to improve the vertical profile models. An ozonesonde can validate the vertical profile models of lower altitudes. However, at present, the number of ozonesonde data sets is still limited. To improve our understanding of the distribution and variation of O_3 and water vapor (H_2O) in the tropical troposphere and stratosphere, the Soundings of Ozone and Water in the Equatorial Region/Pacific mission (SOWER/Pacific) has been proposed [*Hasebe et al.*, 1998]. In addition, the Solar Occultation FTS will provide global O_3 vertical profiles for higher attitudes [*H. Nakajima et al.*, 2000]. To prepare the accurate database of O_2 *A* band line parameters and Fraunhofer line spectra, O_2 *A* band absorption spectra were acquired on the ground using a high resolution FTS and a grating spectrometer. This grating spectrometer will be launched on the balloon together with LPMA FTS.

4.8.2. Error transfer estimation

There were many systematic error sources both in measurement and in model calculation, as summarized in Table 4-13. Most of the errors can be minimized after careful validation and calibration since satellite observation is very stable, frequent, and long-term. In addition, characteristics of clouds and aerosols can be retrieved by applying the newly studied retrieval algorithm. The vertical profile error of temperature profile and the surface albedo error remain as major sources, the effect of which must be estimated. Figure 4-63 contains a summary of the error sources and the expected accuracy of the retrieved physical parameters.

Table 4-14 shows the scenarios of error analysis a summary of input parameters, error levels, and error sources.

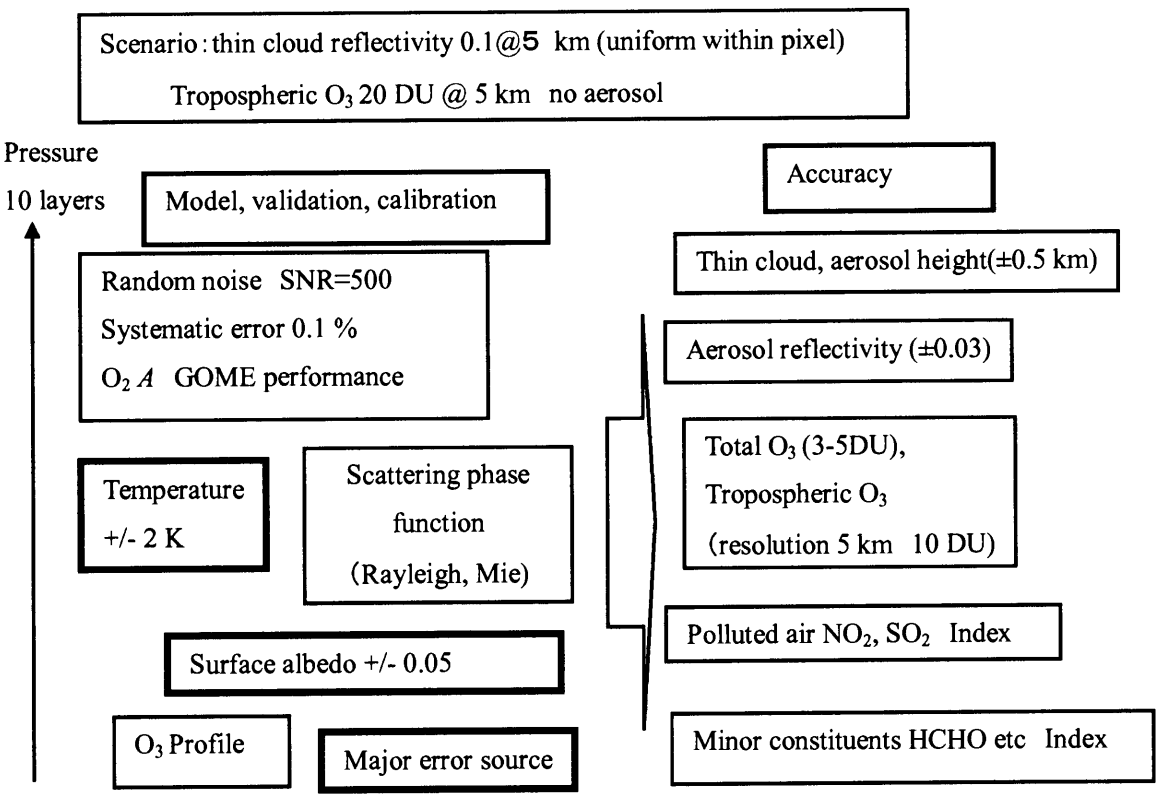

Figure 4-63. Summary of error sources and expected accuracy of the retrieved physical parameters.

Table 4-14. The scenarios of error analysis: a summary of input parameters, error levels, and error sources.

Scenarios			Clear Sky	Tropospheric O_3	Partially covered thick cloud	Fully covered thin cloud	Fully covered Aerosol
Surface type			Ocean	Land	Land	Land	Land
Parameters to be retrieved () error level after retrieval and correction	Total O_3		275 DU (+/-3 DU)	275 DU (+/-3 DU)	275 DU (+/-5 DU)	275 DU (+/-4 DU)	275 DU (+/3 DU)
	Tropospheric O_3		No maxima	30 DU @5 km (+/-10DU +/-5 km)	30 DU @5 km (+/-12DU +/-5 km)	30 DU @5 km (+/-11DU +/-5 km)	30 DU @5 km (+/-11DU +/-5 km)
	Thick Clouds	Altitude	N.A.	N.A.	5 km (+/-0.5 km) *	N.A.	N.A.
		Coverage (with 2 dimensional imager	N.A.	N.A.	0.5 (+/- 0.02)*	N.A.	N.A.
	Thin cloud	Altitude	N.A.	N.A.	N.A.	5 km * (+/-0.5 km)	N.A.
		Reflectivity	<0.01	<0.01	<0.01	0.05 (+/- 0.03)*	<0.01
	Aerosol	Altitude	N.A.	N.A.	N.A.	N.A.	5 km (+/-0.5 km)*
		Reflectivity at 760 nm	<0.01	<0.01	<0.01	<0.01	0.05 (+/- 0.03)*
		Radius (type)	N.A.	N.A.	N.A.	N.A.	0.4 μm dust carbon **
		Optical thickness	N.A.	N.A.	N.A.	N.A.	+/- 0.5
	SO_2 NO_2		Index	Index	Index	Index	Index
	HCHO		Index	Index	Index	Index	Index
Error source	SNR		500	500	500	500	500
	Instrument unknown systematic error after calibration		<0.1%	<0.1%	<0.1%	<0.1%	<0.1%
Uncertainty	Surface Albedo	UV	+/- 1%	+/- 2%	+/- 2%	+/- 2%	+/- 2%
		At 760nm	+/- 2%	+/- 5%	+/- 5%*	+/- 5%*	+/- 5%
	Temperature vertical profile		+/- 2 K*	+/- 2 K*	+/- 2 K *	+/- 2 K *	+/- 2 K
	O_3 vertical profile model (Umkehr layer 5 and 6 (225-35 km))		+/- 10% *	+/- 10% *	+/- 10% *	+/- 10% *	+/- 10% *

* error sources that degrade total O_3 retrieval accuracy

** radius can not be retrieved in case of other type than dust and carbon

4.9. Conclusion of this Chapter

The UV spectrometer discussed in this chapter will retrieve more geophysical parameters than TOMS by replacing discrete spectral sampling with continuous sampling, widening the spectral range, and adding cloud

detection radiometer. As the surface albedo is low in UV region, the atmospheric constituent retrieval is not affected by the earth surface. However, for troposphere measurements, cloud and aerosol has to be carefully detected and characterized. By using multiple pairs of O_2 *A* band, which have various optical thickness, both height and albedo of thin cloud and aerosol can be detected. The solar penetration into the earth atmosphere has strong spectral dependency in UV region, the information on cloud and aerosol vertical distribution is important. In addition, dust and carbonaceous aerosols, which is related to human activity, has absorption in UV region. Continuous spectral data can especially helps us distinguish the tropospheric O_3 from the total O_3 by using the spectral dependency of UV solar flux penetration and O_3 absorption cross section. Using O_2 *A* band and shortwave UV spectra, the aerosol height, thickness, type, and radius are characterized. Regarding instrumentation, the higher spectral and spatial resolution will improve the accuracy of the retrieval. In addition, the uniform and stable slit functions will improve the retrieval accuracy of minor constituents, which have fine spectral absorption cross-sections. By applying the above mentioned retrieval algorithm, the total O_3, the tropospheric O_3, and the aerosol characteristics will become near real time products. Other constituents such as SO_2, NO_2, BrO, OClO, and HCHO will be scientific products. A radiative transfer model such as STAR code will be customized for UV application and the vector model (polarization model) will be added to improve the accuracy of the calculations.